nature physics

Article

https://doi.org/10.1038/s41567-024-02420-4

Topological temporally mode-locked laser

Received: 8 May 2023

Accepted: 29 January 2024

Published online: 01 March 2024

Check for updates

Christian R. Leefmans[1], Midya Parto[2], James Williams[2], Gordon H. Y. Li[1], Avik Dutt[3,4], Franco Nori[5,6,7] & Alireza Marandi[1,2]

Mode-locked lasers play a crucial role in modern science and technology. They are essential to the study of ultrafast and nonlinear optics, and they have applications in metrology, telecommunications and imaging. Recently, there has been interest in studying topological phenomena in mode-locked lasers. From a fundamental perspective, such study promises to reveal nonlinear topological physics, and from a practical perspective it may lead to the development of topologically protected short-pulse sources. Despite this promising outlook, the interplay between topological photonic lattices and laser mode-locking has not been studied experimentally. In this work, we theoretically propose and experimentally realize a topological temporally mode-locked laser. We demonstrate a nonlinearity-driven non-Hermitian skin effect in a laser cavity and observe the robustness of the laser against disorder-induced localization. Our experiments demonstrate fundamental point-gap topological physics that was previously inaccessible to photonics experiments, and they suggest potential applications of our mode-locked laser to sensing, optical computing and robust topological frequency combs. The experimental architecture employed in this work also provides a template for studying topology in other mode-locked photonic sources, including dissipative cavity solitons and synchronously pumped optical parametric oscillators.

Over the past several years, nonlinear topological phenomena have gained prominence in the study of topological photonics[1]. Experimental realizations, including nonlinear Thouless pumps[2] and topological lasers[3–5], have demonstrated that the combination of nonlinearity and topology engenders exotic topological dynamics and may enable the development of topologically robust photonic technologies. Motivated by this success, there have been substantial efforts to incorporate topology into highly nonlinear, mode-locked photonic sources[6–11], including mode-locked lasers and dissipative cavity solitons. Theoretical work in this direction suggests that topological mode-locking could give rise to both exciting nonlinear physics and new topological devices, such as fabrication-tolerant mode-locked lasers[7] and topologically robust frequency combs[12]. However, despite this promising potential, to the best of our knowledge, photonic lattices with nontrivial topological invariants have not been experimentally demonstrated in mode-locked lasers.

Theoretical proposals for topological mode-locking frequently focus on spectral mode-locking, where the amplitudes and phases of the spectral, or longitudinal, modes of a resonator are synchronized by a mode-locking mechanism[13,14]. Many of these proposals incorporate topological lattices either in the form of spatially coupled resonators[9,10,12] or by using frequency synthetic dimensions[6,7]. However, proposals for topological mode-locking in spatially coupled resonator arrays require challenging fabrication processes, which may make them difficult to realize and to scale in size. On the other hand, proposals for topological mode-locking in frequency synthetic dimensions encounter the challenges of realizing controllable boundary conditions[15] and inhomogeneous couplings[16], which could limit the

[1]Department of Applied Physics, California Institute of Technology, Pasadena, CA, USA. [2]Department of Electrical Engineering, California Institute of Technology, Pasadena, CA, USA. [3]Department of Electrical Engineering, Stanford University, Stanford, CA, USA. [4]Department of Mechanical Engineering and IPST, University of Maryland, College Park, MD, USA. [5]Theoretical Quantum Physics Laboratory, Cluster for Pioneering Research, RIKEN, Wako, Japan. [6]Center for Quantum Computing, RIKEN, Wako, Japan. [7]Department of Physics, University of Michigan, Ann Arbor, MI, USA. e-mail: marandi@caltech.edu

https://doi.org/10.1038/s41567-024-02420-4

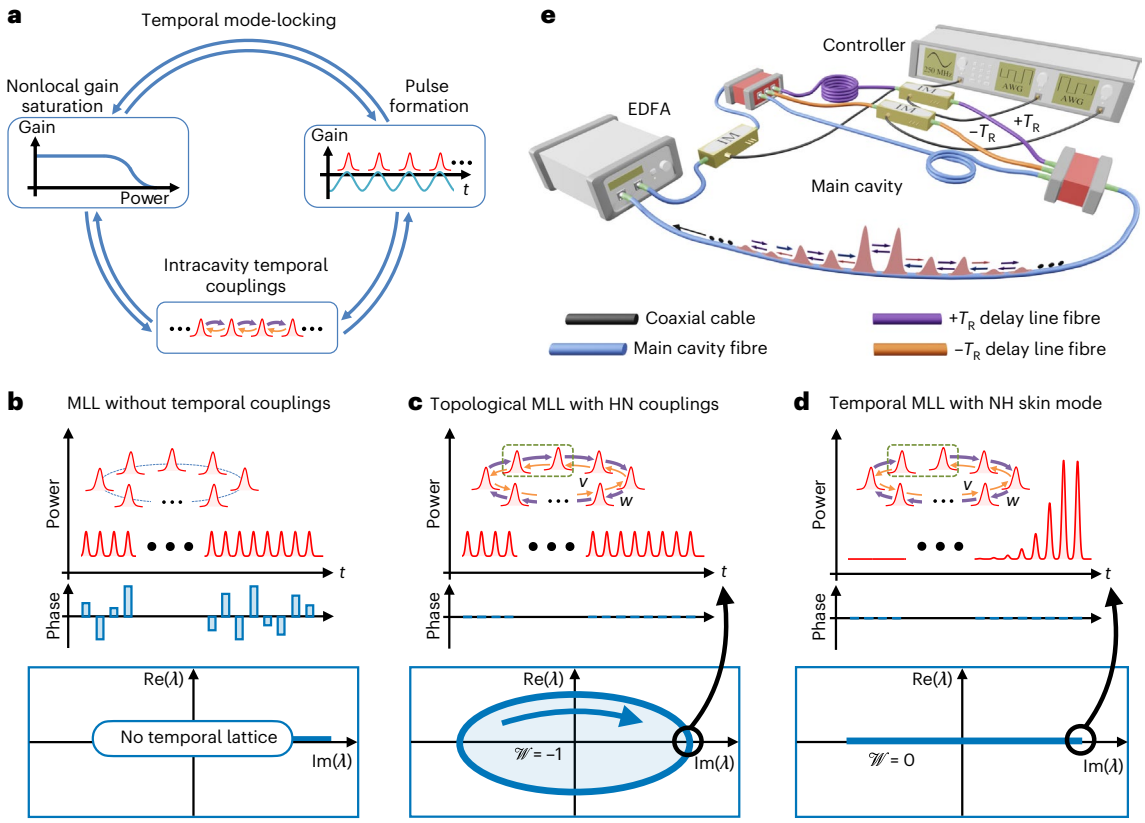

Fig. 1 | Topological temporal mode-locking. a, The constituent elements of temporal mode-locking. **b**, In a harmonically mode-locked laser without temporal mode-locking, the pulse-to-pulse phases may not be correlated. **c**, Intracavity couplings can lock the pulse-to-pulse amplitudes and phases and produce synthetic temporal lattices with nontrivial topology. **d**, Properly engineering the intracavity couplings can reveal non-Hermitian topological phenomena, such as the nonlinearity-driven NHSE studied in this work. Note that, due to the nature of dissipative couplings, Im(λ) appears on the abscissa while Re(λ) appears on the ordinate[17]. **e**, Schematic of the proof-of-principal topological temporally mode-locked laser built for our experiments.

topological physics accessible to these systems. Together, these difficulties motivate the search for an alternative approach to topological mode-locking.

In this work, we overcome the challenges of topological mode-locking in spatial and frequency lattices by theoretically proposing and experimentally demonstrating the topological temporally mode-locked laser. Unlike existing proposals, our topological mode-locked laser leverages the flexibility of temporal synthetic dimensions and relies on the principal of temporal mode-locking, where an additional mode-locking mechanism synchronizes the amplitudes and phases of the temporal modes (that is, pulses) in a harmonically mode-locked laser. By engineering topological couplings between the temporal modes that make up our synthetic lattices, we endow our temporally mode-locked laser with nontrivial topology. Because temporal synthetic dimensions may be used to implement large lattice sizes, multidimensional lattices, inhomogeneous and long-range couplings and tunable boundary conditions, our experimental approach provides a way to access a diversity of topological behaviours in our topological mode-locked system[17,18].

Here we leverage our topological temporally mode-locked laser to demonstrate topological mode-locked lasing in point-gap non-Hermitian topological lattices[19,20]. We first identify a nonlinearity-driven non-Hermitian skin effect[21] (NHSE) that arises due to the nonlocal, nonlinear dynamics of our mode-locked laser. Then we tune the boundary conditions in our mode-locked laser to experimentally connect the existence of a point-gap topological winding number to the existence of the NHSE[22], and we experimentally observe the robustness of the Hatano–Nelson model against disorder-induced localization[23,24]. Our topological temporally mode-locked laser may enable the design of robust frequency combs, while our general temporal mode-locking architecture may have applications to sensing and optical computing (Supplementary Information Sections 7 and 8).

Results

Operating principle and experimental setup

As we illustrate in Fig. 1a, a topological temporally mode-locked laser consists of three basic elements, which are nonlocal gain saturation, a pulse formation mechanism (here, amplitude modulation) and intracavity temporal couplings. A conventional harmonically mode-locked laser possesses the first two of these elements[13], which together give rise to N evenly spaced temporal modes, or pulses, in a laser cavity. While the amplitudes of these pulses are uniform, their phases may drift relative to one another[25] (Fig. 1b). The addition of intracavity couplings stabilizes the relative phases and amplitudes of the pulses, giving rise to what we refer to as temporal mode-locking (Fig. 1c). While simple implementations of temporal mode-locking have been studied previously as a technique to suppress supermode noise in harmonically mode-locked lasers[25–28], here we show that by engineering our intracavity couplings to produce synthetic temporal topological lattices, temporal mode-locking may be used to realize complex nonlinear topological phenomena (Fig. 1c,d).

At sufficiently low powers, where the Kerr nonlinearity may be neglected, the dynamics of our topological temporally mode-locked laser can qualitatively be described by a modified master equation for active mode-locking[13]. This master equation may be approximated as a tight-binding model of the form

https://doi.org/10.1038/s41567-024-02420-4

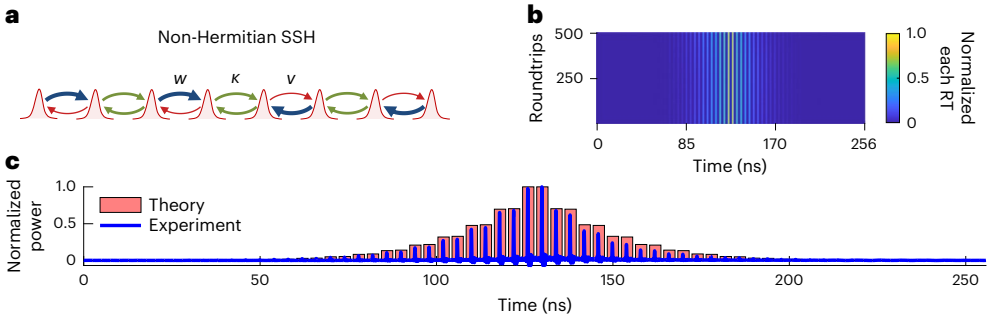

Fig. 2 | Nonlinearity-driven NHSE in a topological mode-locked laser. **a**, Schematic representation of the NH-SSH domain wall implemented in our mode-locked laser's synthetic lattice. **b**, Heat map of our mode-locked laser's output over 500 roundtrips. The pulses are broadened for visibility. **c**, Mode-locked pulse pattern in our topological mode-locked laser. The data is averaged using the procedure described in Supplementary Information Section 3. The theory is the steady state of equation (1).

$$\frac{\partial a_n}{\partial T} = \left(K_n^{\mathrm{L}} a_{n-1} + K_n^{\mathrm{R}} a_{n+1}\right) + \left(g(T) - \Gamma\right) a_n \tag{1a}$$

$$\frac{\partial g}{\partial T} = -\gamma\left(g - g_0 + g\epsilon\textstyle\sum_n |a_n(T)|^2\right). \tag{1b}$$

Here, a_n is the amplitude of the nth pulse (or the nth site of our synthetic lattice), $g(T)$ describes the nonlinear laser gain, g_0 is the small signal gain, Γ is the effective linear loss, $\gamma = T_{\mathrm{RT}}/\tau$ is the ratio of the roundtrip period to the gain relaxation time, ϵ is related to the saturation intensity and K_n^{L} and K_n^{R} describe nearest-neighbour couplings between the pulses in the mode-locked laser.

From equation (1), we observe that the combined nonlinear dynamics of the intracavity couplings and the gain saturation nonlinearity produce temporal mode-locking. Crucially, we assume that the relaxation time of our gain medium is much slower than the roundtrip time of our laser cavity. As a result, the gain saturates only due to the average power in our topological temporally mode-locked laser. In this sense, the gain saturation constitutes a nonlocal nonlinearity that acts equally on all sites a_n in our temporal synthetic lattice. As we show in Supplementary Information Section 4, the result of this nonlocal gain saturation is to drive the pulse amplitudes a_n towards the lowest-loss eigenstate defined by the couplings K_n^{L} and K_n^{R}.

While equation (1) qualitatively describes the dynamics of our topological temporally mode-locked laser at sufficiently low powers, where the Kerr nonlinearity may be neglected, at higher intracavity powers, the Kerr nonlinearity can introduce additional dynamics. We consider the effect of the Kerr nonlinearity in Supplementary Information Section 5.

The fact that at sufficiently low powers the steady state of our topological temporally mode-locked laser tends towards the lowest-loss eigenstate defined by the intracavity couplings makes the topological temporally mode-locked laser well suited to study non-Hermitian point-gap topology. Unlike Hermitian topological lattices, point-gap topological lattices exhibit the NHSE, where all states, including the lowest-loss state, localize near a boundary in the system[21,29]. This enables our topological mode-locked laser to probe the existence of the NHSE in synthetic point-gap topological lattices.

To demonstrate the interplay between point-gap topology and topological temporal mode-locking, in Fig. 1c,d we schematically illustrate topological temporal mode-locking with a Hatano–Nelson lattice[23,24], which consists of a one-dimensional chain with asymmetric couplings w and v. In the presence of periodic boundary conditions, the Hatano–Nelson model exhibits a topologically nontrivial winding around a reference point in the complex energy plane[20], which can be associated with a topological winding number $\mathcal{W}$. In this case, we expect the temporal structure in our laser to possess uniform amplitudes and phases because of the lattice's translational symmetry (Fig. 1c). On the other hand, in the presence of open boundary conditions (Fig. 1e), the eigenvalues of the Hatano–Nelson model collapse onto a line, the lattice's topological winding number becomes trivial[19] and the mode-locked temporal structure becomes strongly localized near the boundary. It is important to note that, although this NHSE occurs in the topologically trivial phase, it is a distinctly topological phenomenon, in the sense that it both guarantees and is guaranteed by the presence of a topological invariant in the bulk lattice[22].

To experimentally realize a topological temporally mode-locked laser, we construct the system presented in Fig. 1e. This proof-of-principle temporally mode-locked laser consists of a fibre cavity ($T_{\mathrm{RT}} = 256$ ns) and two optical delay lines, which are responsible for implementing nearest-neighbour dissipative couplings between the laser's temporal modes. A commercial erbium-doped fibre amplifier (EDFA) provides the system's nonlocal gain saturation ($T_{\mathrm{RT}}/\tau \approx 10^{-5}$), while we sinusoidally modulate an intensity modulator in the main cavity to generate $N = 64$ mode-locked pulses with widths of ~100 ps and a repetition period of $T_{\mathrm{R}} = 4$ ns. Additional intensity modulators in the optical delay lines control the coupling strengths between the pulses and enable us to dynamically tune both the lattice model under study, as well as the boundary conditions of our synthetic lattice. Notably, because each delay line controls only one direction of the coupling between two pulses, it is straightforward to realize non-Hermitian topological lattice models in our system[17].

Topological mode-locking at a non-Hermitian domain wall

To demonstrate topological temporal mode-locking, we first observe a nonlinearity-driven NHSE in a non-Hermitian Su-Schrieffer-Heeger (NH-SSH) lattice[30,31]. While the point-gap topological winding number of this lattice is trivial, the observed nonlinearity-driven NHSE arises due to the nontrivial point-gap topology of the bulk NH-SSH lattice[32]. We begin by tuning our EDFA gain to achieve a small signal gain of ~23.1 dB, which, in the presence of the NH-SSH domain wall, results in an output power of ~42 μW. At first, we operate our laser with homogeneous nearest-neighbour couplings, so that our laser supports a train of 64 mode-locked pulses. We then switch the intracavity couplings in our mode-locked laser to implement the NH-SSH domain wall illustrated in Fig. 2a. Shortly after, the pulse pattern in the laser forms a skin mode at the domain wall of the synthetic NH-SSH lattice (Fig. 2a,b). While the exact pulse pattern fluctuates slightly due to instabilities in the laser, we find that the distribution of the pulse intensities exhibits excellent agreement with the lowest-loss eigenstate of the theoretical NH-SSH lattice, in accordance with equation (1).

While domain-wall skin modes have been observed previously in linear photonic lattices[32,33], the dynamics that drive skin mode formation in our topological mode-locked laser are unambiguously different.

https://doi.org/10.1038/s41567-024-02420-4

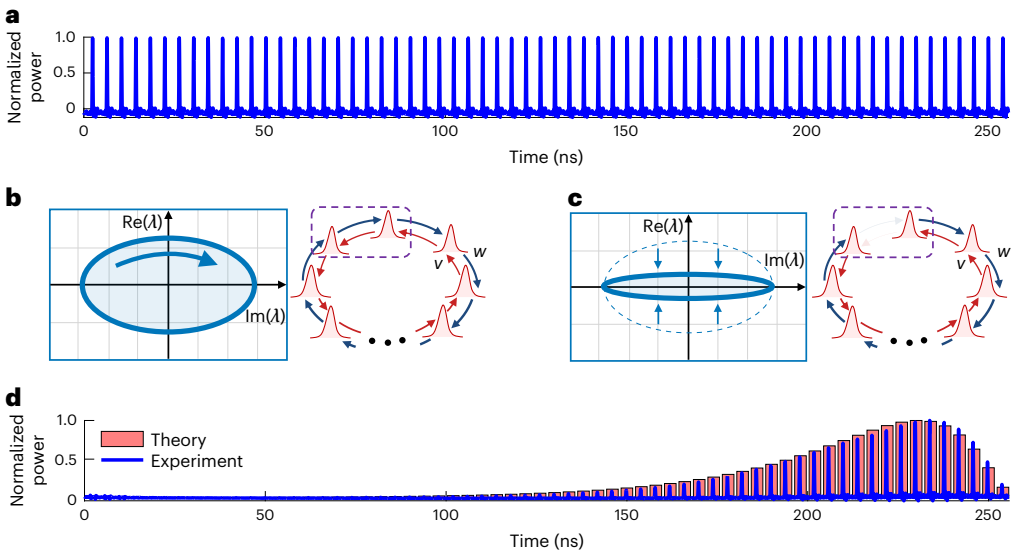

Fig. 3 | Topological winding in a topological mode-locked laser. a, Mode-locked pulse pattern in a Hatano–Nelson lattice with periodic boundary conditions. **b**, This lattice possesses a nontrivial topological winding number. **c**, Schematic of a Hatano–Nelson lattice with partially open boundary conditions. The change in the eigenvalues is exaggerated for illustrative purposes. **d**, With the boundary present, we observe a nascent skin mode, which provides experimental evidence of the nontrivial topological winding number in the bulk Hatano–Nelson lattice. The plots in **a** and **d** are generated from the data in Extended Data Fig. 1 using the averaging procedure discussed in Supplementary Information Section 3.

In linear photonics experiments, skin modes form due to random walks on conservatively coupled lattices with asymmetric couplings. In stark contrast, skin modes in our laser form due to the combined nonlinear dynamics of our laser's nonlocal gain saturation and dissipative, intracavity couplings. Unlike in the linear regime, where an external excitation is required to see skin mode formation, the nonlinear dynamics of our system enable skin modes to form spontaneously within our system. Moreover, while the skin modes in linear systems inevitably decay due to intrinsic losses, the net gain in our system supports the skin modes as long as our laser is stable. Because of the radically different dynamics that govern the skin modes in our system, we refer to skin mode formation in our laser as a nonlinearity-driven NHSE.

Tuning the boundary conditions of the Hatano–Nelson model

We next investigate the sensitivity of the Hatano–Nelson model to its boundary conditions by dynamically tuning the boundary conditions of the temporal synthetic lattice in our topological mode-locked laser. As the occurrence of the NHSE both guarantees and is guaranteed by the existence of a nontrivial topological winding number[22], this experiment confirms the existence of a nontrivial topological winding number in our Hatano–Nelson lattice with periodic boundary conditions.

We first tune our EDFA to operate with a small signal gain of ~22.2 dB, and we program our delay line couplings to implement the Hatano–Nelson model with $w/v = \sqrt{2}$ and periodic boundary conditions (Fig. 3b). In this case, our laser emits a uniform pulse train, as we would expect from translation symmetry (Fig. 3a). Next, we dynamically reduce the coupling at the boundary of the Hatano–Nelson lattice (Fig. 3c). After a series of relaxation oscillations, the pulse pattern in the laser localizes near the new boundary (Fig. 3d). While the finite extinction ratio of our delay line intensity modulators prevents us from achieving perfect open boundary conditions, the observed nascent skin mode presages the skin mode that emerges in the presence of perfect open boundary conditions. From this nascent skin mode, we conclude that the Hatano–Nelson lattice implemented with periodic boundary conditions in our topological temporally mode-locked laser possesses a nontrivial topological winding number.

The sensitivity of point-gap topological lattices to their boundary conditions is a key feature of systems like the Hatano–Nelson model. However, previous photonic architectures, whether in the spatial[34], frequency[35], or temporal domains[32,33], have not demonstrated the control necessary to dynamically introduce a boundary in a periodic lattice. The fact that we can accomplish this in our topological temporally mode-locked laser highlights the fact that, in addition to producing a nonlinearity-driven skin effect, our topological temporally mode-locked laser enables the study of fundamental non-Hermitian topology that has not been realized on existing photonic platforms. Moreover, the observed sensitivity of our laser's pulse pattern to the boundary conditions of the Hatano–Nelson model suggests the possibility that our temporally mode-locked laser may be used for sensing. We explore this possibility in Supplementary Information Section 8.

Robustness of the Hatano–Nelson model

Having established that the Hatano–Nelson lattice exhibits a nontrivial topological invariant in our mode-locked laser, we next verify that it exhibits robustness against disorder. Unlike trivial Hermitian one-dimensional lattices, where any degree of disorder causes localization in the thermodynamic limit[36,37], the Hatano–Nelson model displays robustness against disorder-induced localization[24]. It is believed that this robustness originates from the Hatano–Nelson model's nontrivial topology[19]. In the present experiments, we observe the Hatano–Nelson model's robustness against disorder-induced localization and verify that it occurs in the presence of a nontrivial topological invariant (Fig. 4).

We begin by programming the couplings of our laser to implement the Hatano–Nelson model with periodic boundary conditions and $w/v = \sqrt{2}$, and we add non-Hermitian coupling disorder distributed according to Unif$(0, 0.2w)$ to each direction of each coupling (Fig. 4a). In the presence of this strong disorder, we observe that the resulting pulse pattern in our mode-locked laser is nonuniform but still distributed throughout the lattice. We then introduce a boundary into the Hatano–Nelson lattice (Fig. 4b). In the presence of the boundary, the pulse pattern in the laser forms a nascent skin mode, which establishes that the disordered Hatano–Nelson lattice with periodic boundary conditions still possesses a nontrivial winding number.

https://doi.org/10.1038/s41567-024-02420-4

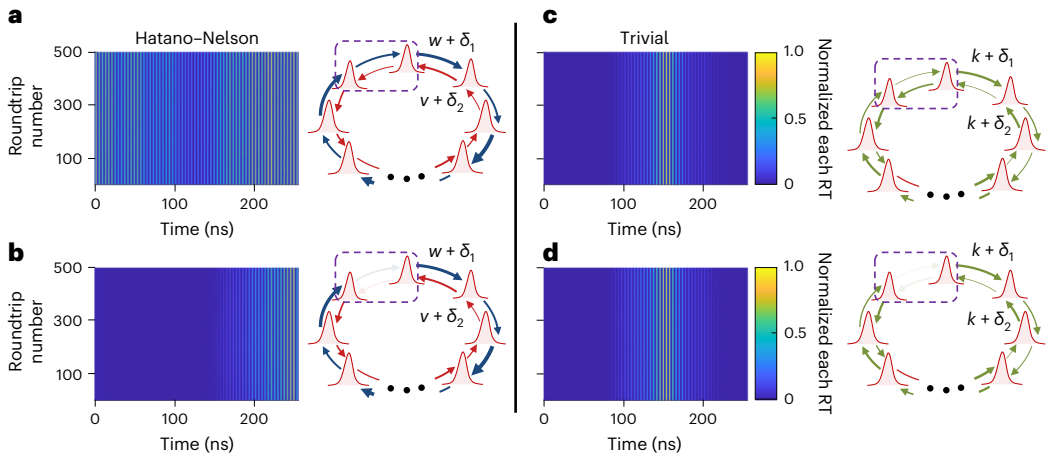

Fig. 4 | Robustness against disorder-induced localization. a, Mode-locked pulse pattern of a disordered Hatano–Nelson lattice with periodic boundary conditions. **b**, A nascent skin mode emerges upon introducing a boundary in the Hatano–Nelson lattice, which provides evidence of the system's robustness against disorder-induced localization. **c**, Mode-locked pulse pattern in a disordered trivial lattice with periodic boundary conditions. **d**, The pulse pattern is essentially unchanged in the corresponding lattice with a boundary. In the lattice schematics depicted in **a**, **b**, **c** and **d**, δ_1 and δ_2 represent the addition of the non-Hermitian coupling disorder described in the text. The pulses in **a**, **b**, **c** and **d** are broadened for improved visibility.

Moreover, it is known that this sensitivity of the Hatano–Nelson model to the boundary conditions is an indication that the system with periodic boundary conditions is in a delocalized phase[23,24].

To contrast the behaviour of the disordered Hatano–Nelson lattice with that of a trivial lattice, we repeat the experiment above with a trivial Hermitian lattice. In this case, we find that, barring finite size effects (Supplementary Information Section 6), the pulse pattern observed in our mode-locked laser appears nearly identical in both the periodic lattice and in the lattice with a boundary (Figs. 4c,d). The lack of this system's sensitivity to the boundary conditions indicates that it has entered a localized phase.

Our robustness measurement is notable in several ways. First, the robustness of the Hatano–Nelson model's topological phase has not been demonstrated before in photonic systems, as previous photonic studies of point-gap topology have not implemented the Hatano–Nelson lattice with periodic boundary conditions. Second, our robustness measurement utilizes off-diagonal non-Hermitian disorder. Given recent theoretical interest in non-Hermitian disorder[38,39] and recent photonic demonstrations of diagonal non-Hermitian disorder[40,41], our realization of off-diagonal non-Hermitian disorder provides an exciting direction for future study. Finally, the robustness of the Hatano–Nelson lattice in our laser may provide a path for realizing robust topological frequency combs. We investigate this possibility in Supplementary Information Section 7.

Phase synchronization

Up to this point, our measurements have focused on the intensity patterns that form in our topological temporally mode-locked laser. However, equation (1) predicts that the temporal couplings in our laser should determine the relative phases of the pulses in our laser, in addition to their relative amplitudes. To verify this, we construct a topological temporally mode-locked laser that supports 69 pulses separated by $T_{R2} = 8$ ns. The system possesses a single $+T_{R2}$ delay line, which enables the topological temporally mode-locked laser to implement unidirectional Hatano–Nelson couplings with periodic boundary conditions. We send the output of this laser to the optical hybrid setup depicted in Fig. 5a, which measures the relative phases between each pulse and its nearest neighbours in the mode-locked laser.

To begin our experiments, we first disconnect the $+T_{R2}$ delay line and operate our system as a traditional harmonically mode-locked laser without temporal couplings. In this case, we expect each pulse in our mode-locked laser to form independently, and we expect the pulse-to-pulse phases to be uncorrelated. Indeed, while the amplitudes of the measured pulses are relatively uniform (Fig. 5b), the pulse-to-pulse phases appear to vary randomly (Fig. 5c). This situation changes dramatically once we reconnect the $+T_{R2}$ delay line. In the presence of the topological temporal couplings, the measured pulse amplitudes remain relatively uniform, but now the pulse-to-pulse phases become synchronized, as we would expect from equation (1). This verifies that topological temporal mode-locking controls the pulse-to-pulse phases of a pulse train, in addition to the pulse-to-pulse amplitudes.

Outlook

In summary, we have theoretically proposed and experimentally demonstrated the topological temporally mode-locked laser. Our demonstration overcomes the challenges faced by many of the existing theoretical proposals for topological mode-locking by utilizing temporal synthetic dimensions and the principal of temporal mode-locking. We use our topological mode-locked laser to study a novel nonlinearity-driven NHSE and to study the Hatano–Nelson model under different boundary conditions. We verify the existence of the Hatano–Nelson model's nontrivial topological invariant in our laser, and we observe this model's robustness against disorder-induced localization.

Our observation that the pulse pattern in our laser is sensitive to the boundary conditions of the Hatano–Nelson model suggests our laser may find use as a sensor, while our topological robustness measurement suggests that topological temporal mode-locking may provide a route to build topologically robust frequency combs. We explore these potential applications in Supplementary Information Sections 7 and 8. Moreover, the fact that we can measure pulse patterns that agree well with the predictions of equation (1) suggests that our temporally mode-locked laser may also provide a mechanism to physically compute eigenvectors.

Beyond these potential applications, the temporal mode-locking architecture demonstrated in this work provides promising directions for future work in nonlinear topological photonics. Due to the flexibility of our intracavity couplings, our temporally mode-locked laser may be adapted to study exciting phenomena such as higher-dimensional NHSEs[42], point-gap topological models with long-range couplings[35] and non-Hermitian topological Anderson insulators[41]. Moreover, this

https://doi.org/10.1038/s41567-024-02420-4

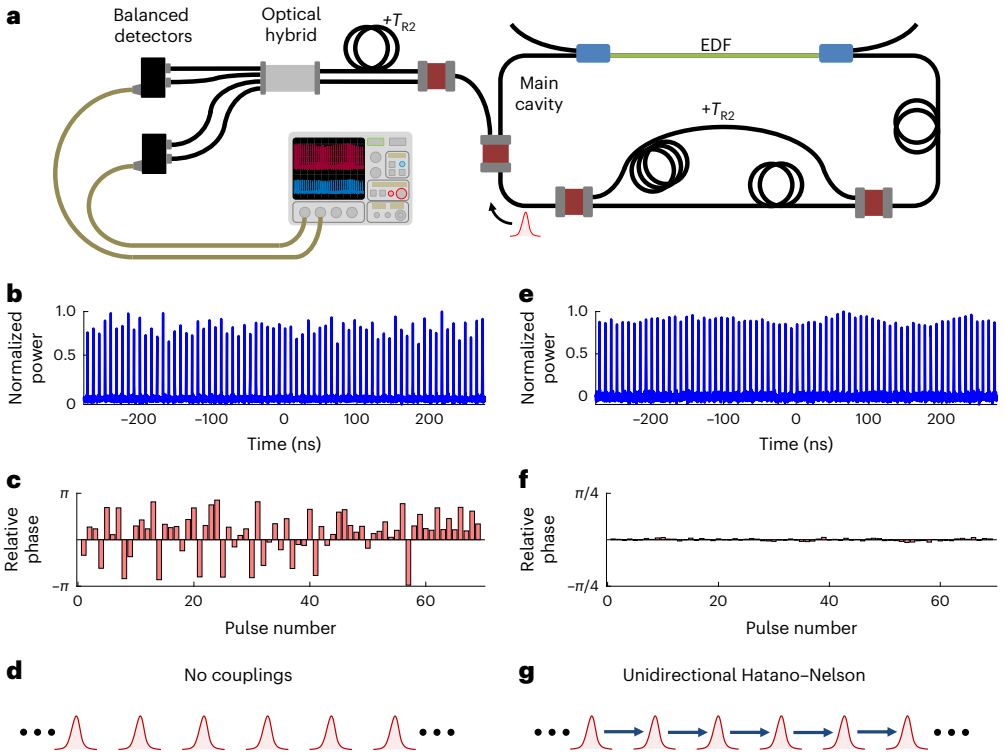

Fig. 5 | Robustness against disorder-induced localization. a, Schematic of the optical hybrid setup used to measure the pulse-to-pulse phases. **b**, Pulse intensities measured on a single roundtrip of a traditional harmonically mode-locked laser. **c**, Pulse-to-pulse phases corresponding to the pulses measured in **b**. **d**, Schematic representation of the pulses in a harmonically mode-locked laser without temporal couplings. **e**, Pulse intensities measured on a single roundtrip of a topological temporally mode-locked laser with unidirectional Hatano–Nelson couplings. The pulse trains in **b** and **e** are measured using a photodetector not depicted in **a**. **f**, Pulse-to-pulse phases corresponding to the pulses measured in **e**. Note that each bar in **c** and **f** represents the phase of a pulse in **b** or **e** relative to its subsequent nearest neighbour. The final bars in **c** and **f** represent the phases of the last pulses in **b** and **e** relative to the first pulses on the next roundtrip. **g**, Schematic representation of a Hatano–Nelson lattice with unidirectional couplings. EDF, Erbium-doped fibre.

same architecture may also be adapted to study topology in other mode-locked photonic sources, including synchronously pumped optical parametric oscillators[43–45] and dissipative Kerr cavities[46]. In future work, we will investigate topological phenomena in these other mode-locked photonic sources.

Online content

Any methods, additional references, Nature Portfolio reporting summaries, source data, extended data, supplementary information, acknowledgements, peer review information; details of author contributions and competing interests; and statements of data and code availability are available at https://doi.org/10.1038/s41567-024-02420-4.

References

1. Smirnova, D., Leykam, D., Chong, Y. & Kivshar, Y. Nonlinear topological photonics. *Appl. Phys. Rev.* **7**, 021306 (2020).
2. Jürgensen, M., Mukherjee, S. & Rechtsman, M. C. Quantized nonlinear Thouless pumping. *Nature* **596**, 63–67 (2021).
3. Parto, M. et al. Edge-mode lasing in 1D topological active arrays. *Phys. Rev. Lett.* **120**, 113901 (2018).
4. Bandres, M. A. et al. Topological insulator laser: experiments. *Science* **359**, eaar4005 (2018).
5. Contractor, R. et al. Scalable single-mode surface-emitting laser via open-Dirac singularities. *Nature* **608**, 692–698 (2022).
6. Longhi, S. Non-Hermitian topological phase transition in *PT*-symmetric mode-locked lasers. *Opt. Lett.* **44**, 1190–1193 (2019).
7. Yang, Z. et al. Mode-locked topological insulator laser utilizing synthetic dimensions. *Phys. Rev. X* **10**, 011059 (2020).
8. Zykin, A. Y., Skryabin, D. V. & Kartashov, Y. V. Topological solitons in arrays of modelocked lasers. *Opt. Lett.* **46**, 2123 (2021).
9. Tusnin, A. K., Tikan, A. M. & Kippenberg, T. J. Dissipative Kerr solitons at the edge state of the Su-Schrieffer-Heeger model. *J. Phys. Conf. Ser.* **2015**, 012159 (2021).
10. Tikan, A. et al. Protected generation of dissipative Kerr solitons in supermodes of coupled optical microresonators. *Sci. Adv.* **8**, eabm6982 (2022).
11. Fan, Z., Puzyrev, D. N. & Skryabin, D. V. Topological soliton metacrystals. *Commun. Phys.* **5**, 248 (2022).
12. Mittal, S., Moille, G., Srinivasan, K., Chembo, Y. K. & Hafezi, M. Topological frequency combs and nested temporal solitons. *Nat. Phys.* **17**, 1169–1176 (2021).
13. Haus, H. A. Mode-locking of lasers. *IEEE J. Sel. Top. Quant.* **6**, 1173–1185 (2000).
14. Kippenberg, T. J., Gaeta, A. L., Lipson, M. & Gorodetsky, M. L. Dissipative Kerr solitons in optical microresonators. *Science* **361**, eaan8083 (2018).
15. Dutt, A. et al. Creating boundaries along a synthetic frequency dimension. *Nat. Commun.* **13**, 3377 (2022).
16. Li, G. et al. Direct extraction of topological Zak phase with the synthetic dimension. *Light Sci. Appl.* **12**, 81 (2023).
17. Leefmans, C. et al. Topological dissipation in a time-multiplexed photonic resonator network. *Nat. Phys.* **18**, 442–449 (2022).
18. Parto, M., Leefmans, C., Williams, J., Nori, F. & Marandi, A. Non-Abelian effects in dissipative photonic topological lattices. *Nat. Commun.* **14**, 1440 (2023).
19. Gong, Z. et al. Topological phases of non-Hermitian systems. *Phys. Rev. X* **8**, 031079 (2018).
20. Kawabata, K., Shiozaki, K., Ueda, M. & Sato, M. Symmetry and topology in non-Hermitian physics. *Phys. Rev. X* **9**, 041015 (2019).

21. Yao, S. & Wang, Z. Edge states and topological invariants of non-Hermitian systems. *Phys. Rev. Lett.* **121**, 086803 (2018).
22. Zhang, K., Yang, Z. & Fang, C. Correspondence between winding numbers and skin modes in non-Hermitian systems. *Phys. Rev. Lett.* **125**, 126402 (2020).
23. Hatano, N. & Nelson, D. R. Vortex pinning and non-Hermitian quantum mechanics. *Phys. Rev. B* **56**, 8651–8673 (1997).
24. Hatano, N. & Nelson, D. R. Non-Hermitian delocalization and eigenfunctions. *Phys. Rev. B* **58**, 8384–8390 (1998).
25. Quinlan, F., Ozharar, S., Gee, S. & Delfyett, P. J. Harmonically mode-locked semiconductor-based lasers as high repetition rate ultralow noise pulse train and optical frequency comb sources. *J. Opt. A* **11**, 103001 (2009).
26. Harvey, G. T. & Mollenauer, L. F. Harmonically mode-locked fiber ring laser with an internal Fabry–Perot stabilizer for soliton transmission. *Opt. Lett.* **18**, 107–109 (1993).
27. Pottiez, O. et al. Experimental study of supermode noise of harmonically mode-locked erbium-doped fibre lasers with composite cavity. *Opt. Commun.* **202**, 161–167 (2002).
28. Srinivasan, S. et al. Harmonically Mode-locked hybrid silicon laser with intra-cavity filter to suppress supermode noise. *IEEE J. Sel. Top. Quant.* **20**, 8–15 (2014).
29. Bergholtz, E. J., Budich, J. C. & Kunst, F. K. Exceptional topology of non-Hermitian systems. *Rev. Mod. Phys.* **93**, 015005 (2021).
30. Su, W. P., Schrieffer, J. R. & Heeger, A. J. Solitons in polyacetylene. *Phys. Rev. Lett.* **42**, 1698–1701 (1979).
31. Yin, C., Jiang, H., Li, L., Lü, R. & Chen, S. Geometrical meaning of winding number and its characterization of topological phases in one-dimensional chiral non-Hermitian systems. *Phys. Rev. A* **97**, 052115 (2018).
32. Weidemann, S. et al. Topological funneling of light. *Science* **368**, 311–314 (2020).
33. Xiao, L. et al. Non-Hermitian bulk–boundary correspondence in quantum dynamics. *Nat. Phys.* **16**, 761–766 (2020).
34. Liu, Y. G. N. et al. Complex skin modes in non-Hermitian coupled laser arrays. *Light Sci. Appl.* **11**, 336 (2022).
35. Wang, K. et al. Generating arbitrary topological windings of a non-Hermitian band. *Science* **371**, 1240–1245 (2021).
36. Anderson, P. W. Absence of diffusion in certain random lattices. *Phys. Rev.* **109**, 1492–1505 (1958).
37. Longhi, S. Spectral deformations in non-Hermitian lattices with disorder and skin effect: a solvable model. *Phys. Rev. B* **103**, 144202 (2021).
38. Tzortzakakis, A. F., Makris, K. G. & Economou, E. N. Non-Hermitian disorder in two-dimensional optical lattices. *Phys. Rev. B* **101**, 014202 (2020).
39. Luo, X., Ohtsuki, T. & Shindou, R. Universality classes of the Anderson transitions driven by non-Hermitian disorder. *Phys. Rev. Lett.* **126**, 090402 (2021).
40. Weidemann, S., Kremer, M., Longhi, S. & Szameit, A. Coexistence of dynamical delocalization and spectral localization through stochastic dissipation. *Nat. Photon.* **15**, 576–581 (2021).
41. Lin, Q. et al. Observation of non-Hermitian topological Anderson insulator in quantum dynamics. *Nat. Commun.* **13**, 3229 (2022).
42. Song, Y. et al. Two-dimensional non-Hermitian skin effect in a synthetic photonic lattice. *Phys. Rev. Appl.* **14**, 064076 (2020).
43. Roy, A., Parto, M., Nehra, R., Leefmans, C. & Marandi, A. Topological optical parametric oscillation. *Nanophotonics* **11**, 1611–1618 (2022).
44. Roy, A. et al. Temporal walk-off induced dissipative quadratic solitons. *Nat. Photon.* https://doi.org/10.1038/s41566-021-00942-4 (2022).
45. Marandi, A., Wang, Z., Takata, K., Byer, R. L. & Yamamoto, Y. Network of time-multiplexed optical parametric oscillators as a coherent Ising machine. *Nat. Photon.* **8**, 937–942 (2014).
46. Englebert, N., Mas Arabí, C., Parra-Rivas, P., Gorza, S.-P. & Leo, F. Temporal solitons in a coherently driven active resonator. *Nat. Photon.* **15**, 536–541 (2021).

Methods

Experimental setup and calibration

As is shown in Fig. 1e, the topological temporally mode-locked laser studied in this work consists of a main laser cavity and two optical delay lines, which are responsible for introducing nearest-neighbour intracavity couplings between the pulses in the laser. We construct each path from polarization-maintaining patch cables and discrete optical components, which are all terminated in FC/APC connectors to minimize back-reflections. The main cavity contains an EDFA and an intensity modulator, which together produce pulses in the laser cavity. Each of the delay lines also possesses an intensity modulator, which provides reconfigurable pulse-to-pulse control over the intracavity couplings in our laser. The other elements in our temporally mode-locked laser are discussed in Supplementary Information Section 1, where we present a more detailed schematic of our experimental setup.

We calibrate the intracavity couplings in our laser using a multistep procedure. In the first step, we operate below threshold and inject pulses from an auxiliary mode-locked laser, which has the same repetition period as our temporally mode-locked laser, into our laser cavity. We first use these auxiliary pulses to set the length of the main cavity and to synchronize the lengths of the main cavity and the delay lines. Then, we disconnect the feedback in the main cavity path and, one at a time, analyse the throughput of the optical delay lines on a fast photodetector. We send a burst of constant amplitude pulses through the delay lines and apply an RF voltage sweep to the intensity modulators. We use the observed photodetector signal to plot the throughput optical power as a function of the RF voltage, and from this curve we generate preliminary coupling waveforms for our experiments.

We next attempt to overlap the positions of the pulses generated in our laser cavity with those of the auxiliary pulses injected into the cavity. Still operating below the threshold, we use a 10 MHz reference from our auxiliary mode-locked laser as a clock for the RF function generator that drives the main cavity's intensity modulator. We then set the frequency of the function generator's sinusoidal output to be the same as that of the auxiliary mode-locked laser. Finally, we use an RF phase shifter to adjust the phase of the amplitude modulation in the main cavity until we minimize the loss experienced by the auxiliary pulses as they resonate within the cavity. By doing this, our goal is that the pulses generated in our laser will localize in the positions occupied by the auxiliary pulses and therefore experience the same intensity modulator response functions in the delay lines.

The next step in our calibration procedure is to verify that our calibration remains valid once we bring our laser above threshold. To do this, we remove the auxiliary pulses and disconnect the delay lines so that they no longer couple back to the main cavity. We bring the laser above threshold, and we tune the length of the main cavity slightly until we observe a stable pulse train. We apply our preliminary coupling waveforms to the delay line intensity modulators, and, one at a time, we look at the throughput of the delay lines on a fast photodetector. If the throughput does not agree with the expected couplings, we tune the positions of the optical pulses with our RF phase shifter until the agreement with the desired couplings improves. If small discrepancies persist after this tuning, we manually update the coupling waveform to achieve the desired delay line throughput.

Experimental procedure

To begin our experiments, we first block the free space delays in the two delay lines, and we bring just the main cavity above threshold. We then tune the length of the main cavity and the gain of the EDFA until we observe a train of uniformly spaced mode-locked pulses. We then unblock one delay line at a time, and we attempt to lock the delay lines to constructive interference with the main cavity. After this, we utilize the fact that our laser's threshold is lower with the delay line couplings present to reduce the gain of the EDFA. By reducing the EDFA gain, we aim to reduce the effect of the Kerr nonlinearity on the observed mode-locked pulse patterns.

At this point, our delay lines implement constant, nearest-neighbour couplings between the pulses. However, while the couplings are constant, they need not be Hermitian. When studying the Hatano–Nelson lattice under different boundary conditions, we find it convenient to tune the coupling strength in one delay line to be greater than that in the other, so that we implement the Hatano–Nelson model with periodic boundary conditions upon initializing our laser. We can then produce a boundary in this Hatano–Nelson lattice by reducing the coupling between two pulses with our delay line intensity modulators.

After initializing our laser with constant, nearest-neighbour couplings, we abruptly modify the coupling waveforms applied to the delay line intensity modulators to implement the desired lattice model. We implement these couplings for several minutes at a time, and we detect the pulse pattern emitted by our laser with a fast photodetector. We observe this pulse pattern on a fast oscilloscope along with an auxiliary signal that allows us to establish the position of the pulse pattern in the laser's synthetic lattice. We describe this positioning procedure in the Supplementary Information Section 3.

Data availability

The data used to generate the plots and results in this paper are available on figshare (https://doi.org/10.6084/m9.figshare.25050494). Source data are provided with this paper. All other data that support the findings of this study are available from the corresponding author upon reasonable request.

Code availability

The code used to generate the plots and simulation results in this paper is available from the corresponding author upon reasonable request.

Acknowledgements

We are grateful to K. Vahala and L. Wu for lending equipment useful to this work. We thank D. Nelson and N. Hatano for their comments on this work. The authors acknowledge support from NSF Grants No. 1846273 and 1918549 and AFOSR Award No. FA9550-20-1-0040. F.N. is supported in part by the Office of Naval Research (ONR), Japan Science and Technology Agency (JST) (via the Quantum Leap Flagship Program (Q-LEAP) and the Moonshot R&D Grant No. JPMJMS2061) and the Asian Office of Aerospace Research and Development (AOARD) (via Grant No. FA2386-20-1-4069). We wish to thank NTT Research for their financial and technical support.

Author contributions

C.R.L. and A.M. conceived the idea. C.R.L., A.D. and J.W. constructed the experimental setup. C.R.L. developed the theory, performed the simulations and experiments, and analysed the data. M.P. assisted with the simulations and the experiments. G.H.Y.L. helped to improve the experimental procedures. F.N. provided additional insight and guidance. A.M. supervised the project. All authors discussed the results and contributed to the writing of the paper.

Competing interests

A.M. has a financial interest in PINC Technologies Inc., which is developing photonic integrated nonlinear circuits. The other authors declare no competing interests.

Additional information

Extended data is available for this paper at https://doi.org/10.1038/s41567-024-02420-4.

Supplementary information The online version contains supplementary material available at https://doi.org/10.1038/s41567-024-02420-4.

Correspondence and requests for materials should be addressed to Alireza Marandi.

Peer review information *Nature Physics* thanks the anonymous reviewers for their contribution to the peer review of this work.

https://doi.org/10.1038/s41567-024-02420-4

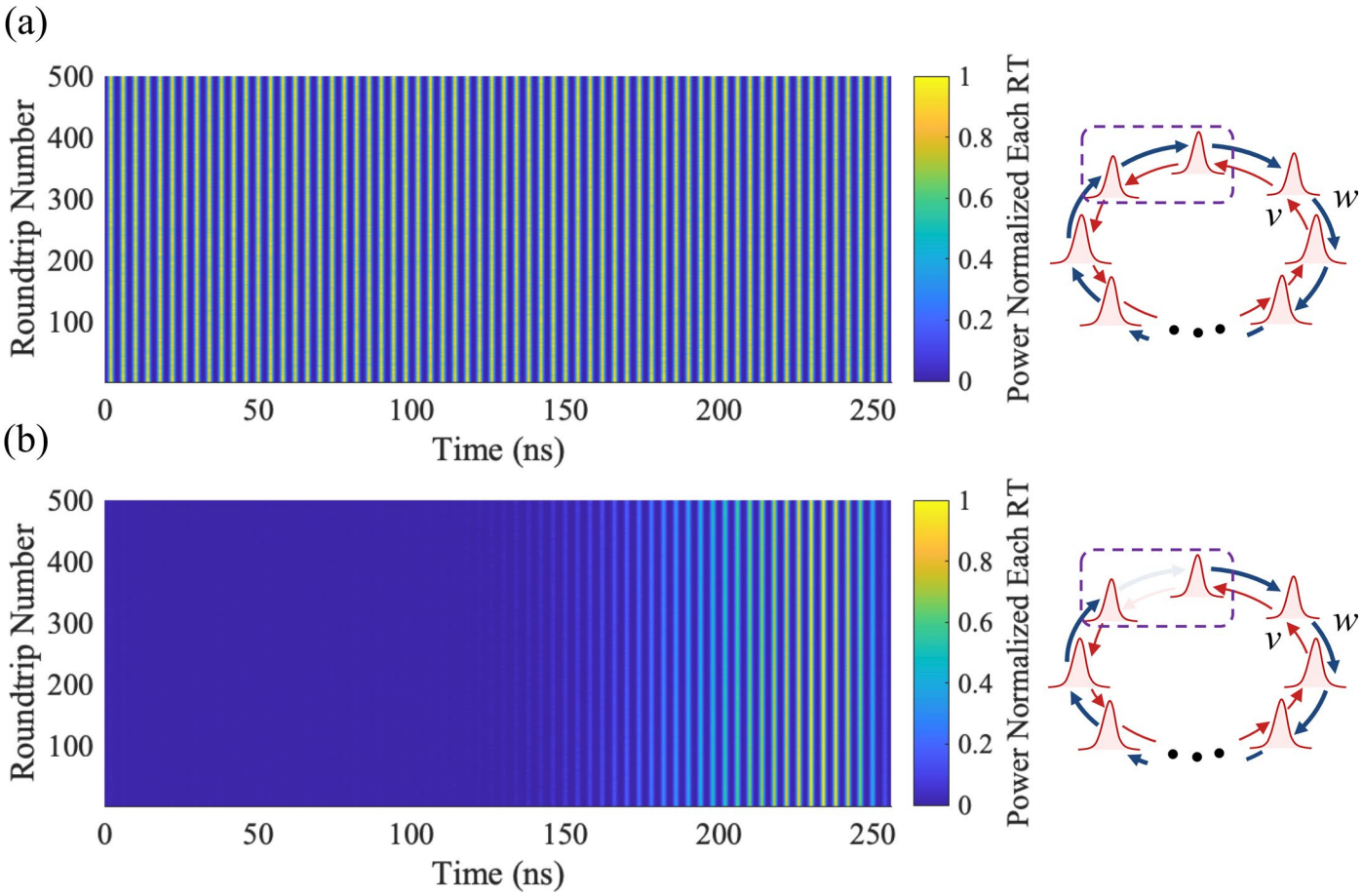

Extended Data Fig. 1 | Topological Temporal Mode-Locking With a Hatano-Nelson Lattice. (a) Heat map of our mode-locked laser's output for 500 roundtrips. Here our laser's intracavity couplings implement the Hatano-Nelson model with periodic boundary conditions. **(b)** A similar heat map, but now where the laser's couplings implement a boundary in the Hatano-Nelson lattice. The data used to generate the heat maps in (a) and (b) are also used to generate the plots in Fig. 3. Note that the pulses in these heat maps are broadened for visibility.